Engineering light emission of two-dimensional materials in both the weak and strong coupling regimes

Research article **Open Access**

Mauro Brotons-Gisbert*, Juan P. Martínez-Pastor, Guillem C. Ballesteros, Brian D. Gerardot and Juan F. Sánchez-Royo*

Engineering light emission of two-dimensional materials in both the weak and strong coupling regimes

DOI 10.1515/nanoph-2017-0041
Received April 5, 2017; revised May 19, 2017; accepted May 24, 2017

Abstract: Two-dimensional (2D) materials have promising applications in optoelectronics, photonics, and quantum technologies. However, their intrinsically low light absorption limits their performance, and potential devices must be accurately engineered for optimal operation. Here, we apply a transfer matrix-based source-term method to optimize light absorption and emission in 2D materials and related devices in weak and strong coupling regimes. The implemented analytical model accurately accounts for experimental results reported for representative 2D materials such as graphene and MoS_2. The model has been extended to propose structures to optimize light emission by exciton recombination in MoS_2 single layers, light extraction from arbitrarily oriented dipole monolayers, and single-photon emission in 2D materials. Also, it has been successfully applied to retrieve exciton-cavity interaction parameters from MoS_2 microcavity experiments. The present model appears as a powerful and versatile tool for the design of new optoelectronic devices based on 2D semiconductors such as quantum light sources and polariton lasers.

Keywords: optical emission enhancement; few layer materials; photoluminescence; MoS_2; graphene; WSe_2; hBN; strong coupling; cavity polaritons; single-photon emitter.

***Corresponding authors: Mauro Brotons-Gisbert and Juan F. Sánchez-Royo,** ICMUV, Instituto de Ciencia de Materiales, Universidad de Valencia, P.O. Box 22085, 46071 Valencia, Spain,
e-mail: Mauro.Brotons@uv.es (M. Brotons-Gisbert); Juan.F.Sanchez@uv.es (J. F. Sánchez-Royo).
http://orcid.org/0000-0001-7254-8292 (M. Brotons-Gisbert)
Juan P. Martínez-Pastor: ICMUV, Instituto de Ciencia de Materiales, Universidad de Valencia, P.O. Box 22085, 46071 Valencia, Spain
Guillem C. Ballesteros and Brian D. Gerardot: Institute of Photonics and Quantum Science, SUPA, Heriot-Watt University, Edinburgh EH14 4AS, UK

1 Introduction

Atomically thin two-dimensional (2D) materials have raised considerable attention in both basic and technological research due to their unique physical properties, such as the observation of the quantum Hall effect, the existence of strong excitonic effects, high carrier mobilities, and the valley and spin polarization [1, 2]. In particular, single layers (SLs) of transition-metal dichalcogenides (TMDs), such as MoS_2, $MoSe_2$, WS_2, and WSe_2, have positioned themselves as strong candidates for 2D optoelectronics, photonics, and the development of valleytronic and photovoltaic devices [3–5] due to their particular electronic properties and strong photoluminescent response [6, 7]. SLs of TMDs have already been used for building transistors, photodetectors, and light-emitting diodes [8, 9]. However, potential applications of 2D materials are not only limited to these technologically relevant fields. Very recently, some 2D materials such as WSe_2 [10–14] and h-BN [15–17] have revealed promising capabilities for the development of new quantum light sources. Crystal structure imperfections or disorder found in these materials can act as efficient carrier trapping centers that behave as sources of single-photon emitters (SPEs). The 2D nature of these SPEs confined to atomically thin materials can, in principle, enhance the photon-extraction efficiency and facilitate a strong and controllable external modification because of the proximity of the SPEs to the material surface. Also, 2D TMDs present strong interaction with light and robust excitons at room temperature. These properties make them extremely interesting for the development of new polaritonic devices operating even at room temperature through the formation of cavity polaritons. In fact, experimental evidence of strong light-matter coupling and the formation of exciton polaritons at room temperature has been recently reported for 2D MoS_2 [18], 2D WS_2 [19], and van der Waals 2D $MoSe_2$/h-BN/$MoSe_2$ heterostructures [20] embedded inside dielectric microcavities.

One of the most significant challenges that must be faced to integrate these 2D materials in competitive optoelectronic, photonic, and quantum devices goes through the optimization of light absorption and emission processes, with the aim to partially compensate their intrinsic low absorption due to their nanoscale thickness. To date, different approaches have been demonstrated to improve light emission in 2D materials. Among these, the use of localized surface plasmon resonances sustained by metal nanoparticles or patterned substrates has appeared to be an effective approach to enhance the photoluminescence (PL) in 2D semiconductors. Plasmonic gold nanorods [21, 22], silica-gold nanoshells [23], and metal nanoantenna-patterned substrates [24–26] have already been used to enhance the PL emission of SLs of 2D TMDs by several orders of magnitude. Recently, a PL enhancement of ~20,000-fold has been achieved for WSe_2 deposited on gold substrates onto which trenches as narrow as sub-20 nm had been patterned [27]. Alternatively, photonic structures have been used to resonantly control and enhance the interaction of light with 2D materials. In this way, the integration of WSe_2 SLs onto a photonic crystal cavity has yielded a PL enhancement of about 60 times [28]. Finally, another intuitive approach used to optically tune the incoupling and outcoupling of light in atomically thin 2D materials has been the modification of their dielectric surroundings. In fact, the Raman signals of graphene [29–31] and 2D TMDs [32–34], as well as the PL signals of 2D TMDs [33, 34], have revealed a strong intensity dependence on the thickness of the underlying silicon dioxide (SiO_2) layer of Si/SiO_2 substrates, due to substrate-related optical interference effects.

The degree of success for these methods to improve light emission of 2D materials relies on the choice of appropriate device structures with optimized characteristics, and, consequently, accurate and versatile design models of optical devices are required. So far, the enhancement of light extraction assisted by surrounding-induced light interferences in 2D materials has been modeled by employing the multiple reflection model [32, 33], with a good concordance with experimental results. However, this model assumes normal incidence of light for both excitation and emission, which limits its applicability for the design of devices in which the angular light emission pattern or the power distribution into guided and leaky modes becomes a relevant parameter. In addition to this, the normal emission approximation would be expected to fail to account for light emission patterns of active 2D materials with vertical emitting dipoles (as would be the case for 2D materials such as InSe [35, 36]). In order to overcome such issues, it is possible to use matrix-based analytical models under the assumption of dipolar nature of optical processes taking place in semiconductors. One of these models, named method of source terms (MST), was proposed by Benisty et al. [37]. This model is based in the combination of a transfer matrix method and a dipole emission source term (see the Supplementary Information for a detailed description of the model), which allows calculating the emission of a thin source plane in an arbitrary planar structure in which the source plane is modeled by incoherent electrical oscillating dipoles. The MST has already been successfully applied to study, design, and characterize top-emitting microcavity light-emitting diodes [38], the coupling of light from an organic light emitting diode (OLED) into a single-mode waveguide [39], the efficient photon extraction from a quantum dot in a broad-band planar cavity antenna [40], and the emission in grating-assisted resonant-cavity light-emitting diodes [41]. Recently, Janisch et al. [42] have developed a different matrix-based method to calculate the angular emission patterns of a single MoS_2 layer evaporated onto Al_2O_3/Al substrates with different thicknesses of Al_2O_3. This method relies on the calculation of the Hertz potential of the nanocavity, from which the electric field distribution along the cavity can be obtained. However, although this Hertz potential-based model allows the calculation of the contribution to the total emitted power by both in-plane and out-of-plane dipoles, information on contributions from TE (s) and TM (p) polarizations is missed. Moreover, in order to take into account the cavity-modified emission rate, additional calculations have to be performed [42]. Opposite to this, the MST allows to calculate the contributions of both TE and TM polarizations on the emission patterns, as well as to calculate the modification of the emission rate in a very straightforward way.

In this work, we evidence the versatility of the MST to study and optimize light emission (PL, Raman) from 2D materials even when these materials are the active component of a device structure and the strong coupling regime is reached. Following the work of Aad et al. [43], we have modified the MST to include the effects of the excitation angle and wavelength, as well as the thickness-related emission intensity variations. The MST has been applied here to a large variety of 2D systems. Graphene has been chosen because of its relevance among 2D materials as a semi-metal. MoS_2 has been chosen as a prototypical 2D TMD semiconductor with strong PL emission. WSe_2 and h-BN have been chosen because of the experimental observation of bright and stable single-photon emission from localized excitons in their 2D forms [10–15, 44]. In the first part of the work, the applicability of the MST has been demonstrated by comparing our calculations

with experimental results available in the literature for MoS_2 and graphene. Motivated by the good agreement observed between calculated and experimental results, in the second part of the work, the MST has been applied for designing multilayer devices using 2D MoS_2 as active material with an optimized response. Also, multilayer structures have been proposed to enhance the extracted photon flux for 2D materials whose dipoles are not necessarily oriented in-plane. In the third part of the work, the MST has been applied to determine the conditions for maximizing the extraction efficiency of SPEs in 2D WSe_2 and h-BN deposited in different substrates. Finally, we go further in the use of MST to simulate angle-resolved PL emission in the strong coupling regime of 2D MoS_2 embedded in a planar optical cavity, from which an anticrossing behavior between the MoS_2 A exciton and the cavity modes is deduced, confirming the formation of exciton polaritons.

2 Optimizing light emission in 2D MoS_2 and graphene

To demonstrate the versatility of the MST to estimate the angular emission patterns of optical processes with dipolar nature, as opposed to multiple reflection models, we present here results of the application of the MST to 2D MoS_2 and graphene. Our results are compared to radiation patterns obtained experimentally by back focal plane (BFP) imaging, which has been demonstrated to be an efficient experimental technique for measuring the emission intensity of active materials as function of the emission angle θ or in-plane photon momentum $k_{||} = k_0 \cdot \sin(\theta)$ [45]. In our calculations, the wavelength dependence and the anisotropy of the refractive indices of the materials have been taken into account. It is worth mentioning that for all calculations presented here, no fitting parameter has been used apart for an overall scaling factor used to match the calculated signal intensities to those experimentally obtained.

It has been demonstrated that the PL from 2D MoS_2 originates solely from in-plane excitons [46]. Therefore, the PL emission of MoS_2 layers can be described by an isotropic distribution of incoherently radiating dipoles lying in planes parallel to the layer interfaces. The thickness-dependent Raman intensity of MoS_2 has been modeled by considering a discrete stacking of dipole sheets, each sheet a SL thick (nominally, 0.6 nm) [6]. Figure 1A shows experimental momentum-resolved TE-polarized (red dotted lines) and TM-polarized (blue dotted lines) PL corresponding to the A exciton of SL MoS_2 deposited onto a glass substrate obtained by BFP imaging, as extracted from Ref. [46]. Calculated values for TE- and TM-polarized PL corresponding to this experimental picture are represented by red and blue solid lines, respectively. A very good agreement between experiment and calculations is observed for both polarizations. Figure 1B shows the x-polarized antenna-like radiation BFP image calculated from the TE and TM components shown in Figure 1A, which also matches that obtained experimentally [46].

The MST can also be employed to calculate the BFP radiation patterns of the G and 2D Raman modes of graphene due to their dipolar nature [47]. In order to analytically model the intensity of the G and 2D Raman modes for graphene, we have considered the sum of two incoherent orthogonal in-plane point dipoles with ratios 1:1 for the

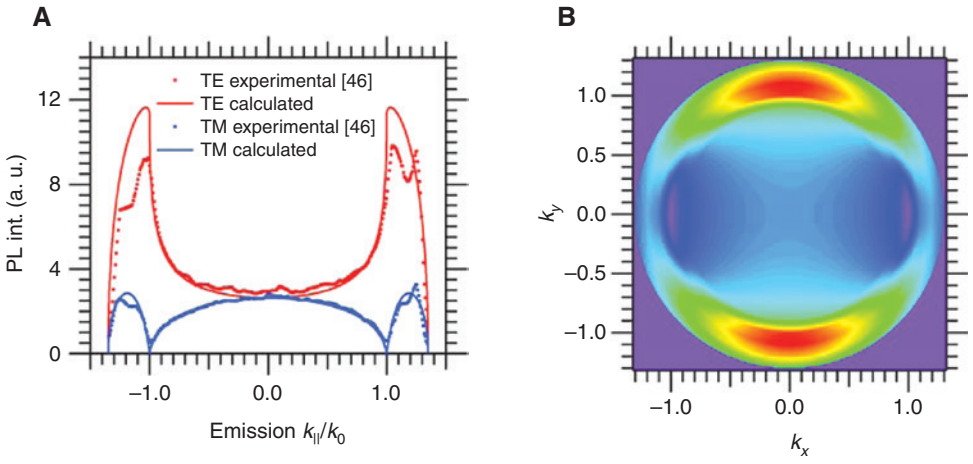

Figure 1: (A) Experimental (dotted lines) and calculated (solid lines) BFP cross-sections for the A exciton PL of SL MoS_2. Experimental data have been obtained from Ref. [46]. (B) Polarized antenna-like radiation BFP image calculated from the TE and TM components shown in (A).

isotropically polarized G band and 3:1 for the polarized 2D band [47]. Figure 2A and B shows experimental TE- and TM-polarized detection BFP profiles (dotted lines) of the G mode of a single-layer graphene deposited onto a glass substrate, obtained from Ref. [47]. The corresponding BFP profiles calculated in the frame of the MST are also shown in Figure 2A and B (solid lines). Figure 2C shows a comparison between the experimental and calculated BFP profiles of the G mode obtained for unpolarized detection. Experimental values have also been extracted from Ref. [47]. Figure 2D and E shows the calculated BFP images of the G mode for polarized and unpolarized detection, respectively. The emission isotropy of the Raman G mode can be observed in Figure 2E. As for the case of MoS_2 PL angular patterns, a good correspondence between experimental and calculated values is observed for the Raman

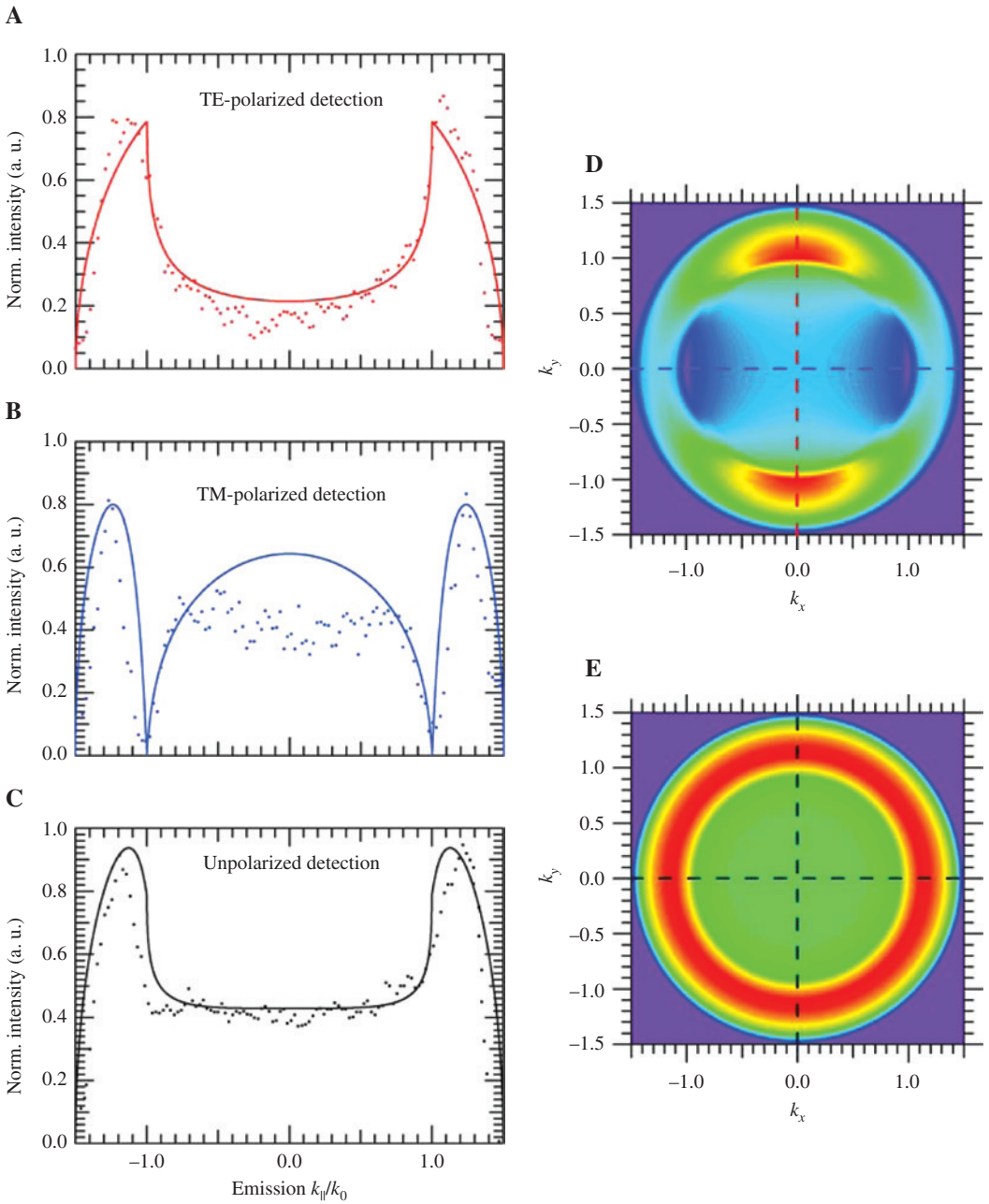

Figure 2: Comparison between experimental (extracted from Ref. [47]) and calculated BFP cross-sections for the Raman G mode of graphene for TE-polarized (A), TM-polarized (B), and unpolarized (C) detection, respectively. Calculated BFP images of the Raman G mode of graphene for polarized (D) and unpolarized (E) detection.

G band of graphene. In addition to these results, the MST has appeared to quantitatively reproduce the anisotropic BFP patterns of the Raman 2D mode of graphene for both polarized and unpolarized detection configurations (see Supplementary Information).

It is worth mentioning that the BFP patterns for the PL of MoS_2 and Raman of graphene can also be calculated by using different analytical models, as shown in Refs. [46, 47], respectively. In Ref. [46], the normalized local density of optical states, the time-averaged populations, and the dipole moments of in-plane and out-of-plane dipoles of a single emitter were taken into account for the simulation of the PL patterns in MoS_2. In Ref. [47], the BFP intensities were calculated by considering the TM- and TE-polarized components of the electric fields radiated by a point dipole on the glass-air interface, depending on its in-plane orientation, the azimuthal and polar emission angles, and the distance from the emitter center [45]. Although both analytical models offer a very good agreement between experimental and calculated values for BFP imaging, it is not straightforward to employ such analytical models to calculate angular emission patterns in multilayered structures in which more than one interface is present. In this sense, the MST offers a clear advantage with respect to those models, as every interface is taken into account by a unique transfer matrix.

Both SiO_2/Si and Al_2O_3/Al substrates are able to tune the PL intensity of top 2D TMDs. The MST also allows us to calculate the total emitted power in the far-field that can be collected by the numerical aperture (NA) of a particular objective, simply by integrating the normalized emitted power density over the corresponding solid angle. Figure 3A and B shows the PL intensity evolution of SL MoS_2 deposited onto SiO_2/Si [33] and Al_2O_3/Al [42] substrates as a function of the SiO_2 and Al_2O_3 thickness, respectively, in which the trend calculated using the MST has been included. In these calculations, the excitation and emission conditions used in the experiments are considered. As can be seen in these figures, there is an excellent agreement between calculated and experimental values. A maximum of PL intensity can be observed for SiO_2 layers of ~330–350-nm thick in both experimental and calculated values. Compared to the minimum PL intensity at ~230 nm SiO_2, there is a ~30-fold increase

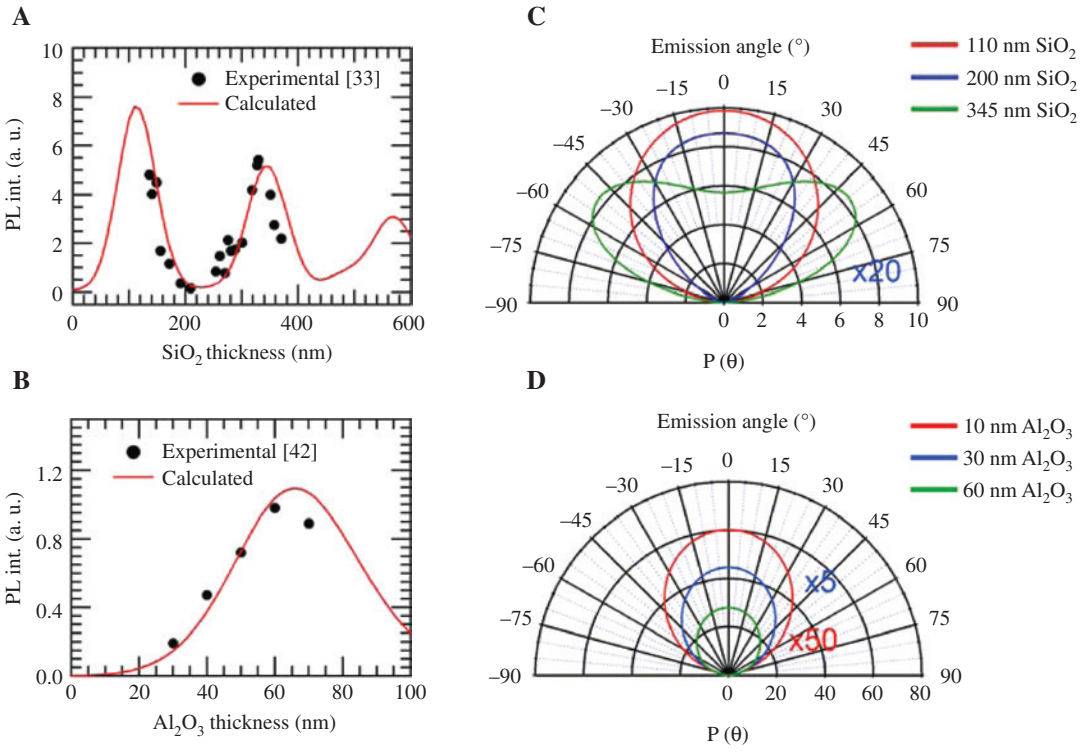

Figure 3: Comparison between experimental and calculated values of the PL intensity of SL MoS_2 deposited onto Si/SiO_2 (A) and Al/Al_2O_3 (B) substrates as function of the SiO_2 and Al_2O_3 thicknesses, respectively. Experimental values have been obtained from Ref. [33] and Ref. [42], respectively. Calculated power radiated per unit solid angle in the far field obtained for underlying SiO_2 layers of 110, 200, and 345 nm of thickness (C), and Al_2O_3 layers of 10, 30, and 60 nm of thickness (D). The colored numbers appearing in Figures (C) and (D) indicate that the corresponding patterns have been multiplied by such factors for comparison purposes.

in the PL intensity with the optimized thickness. Our calculations also indicate that an even higher enhancement of the PL signal can be obtained for underlying SiO_2 layers of ~110 nm, where a ~39-fold increase would be achieved. With regard to MoS_2 sheets on Al_2O_3/Al substrates (Figure 3B), the PL intensity of MoS_2 increases as the Al_2O_3 thickness does, although calculations show that a maximal enhancement is expected for Al_2O_3 layers of ~60–70 nm in thickness. Figure 3C and D shows the simulated power radiated per unit solid angle in the far field obtained for underlying SiO_2 layers of 110, 200, and 345 nm in thickness and Al_2O_3 layers of 10, 30, and 60 nm in thickness, respectively. In these figures, the calculated angular patterns for 200 nm of SiO_2 and 10 and 30 nm of Al_2O_3 have been multiplied by factors of 20, 50, and 5, respectively, for an easier comparison. As can be observed in these figures, both total collected power and angular patterns are affected by the substrate choice.

Results shown in Figure 3A and B evidence the already reported effects of substrate-related optical interference in the PL signals of 2D materials. The origin of such interference effects has been extensively discussed in several 2D systems on the basis of the interference model [32–34]. Within this model and assuming that the PL emission intensity is proportional to the excitation (absorption), the resulting modulation of light emission can be understood as the combination of the optical interference produced in both excitation and emission processes due to the multiple reflections within underlying substrates. In this way, if only absorption or emission process was taken into account rather than a combination of both, interference effects would give rise to absorption or emission maxima (constructive interference) for substrate thicknesses of $d \sim (2m+1)\cdot\lambda/4n$, with m being a positive integer ($m = 0, 1, 2\ldots$), n being the refractive index of the underlying oxide layer, and λ being the excitation or emission wavelength, respectively. Within this picture, the maxima of PL observed in Figure 3A for MoS_2 deposited onto SiO_2/Si substrates (112, 340, and 565 nm) can be interpreted as a combination of absorption (108, 326, and 543 nm) and emission (115, 345, and 575 nm) maxima obtained with an excitation wavelength of 632.8 nm. It is worth mentioning that the dependence of the observed PL intensity observed for SL MoS_2 deposited onto SiO_2/Si and Al_2O_3/Al substrates (Figure 3A and B) is not a general result (position and intensity of maxima), as it depends on the excitation wavelength used in the experiment.

As an extension of these results, Figure S4 (see Supplementary Information) shows that the model also yields very good results for other TMDs such as WSe_2. We note that our results demonstrate that an underlying SiO_2 thickness of ~110 nm is optimum to maximize the luminescent response of the 2D TMDs MoS_2 and WSe_2 when using excitation wavelengths of 532 and 632 nm. Moreover, taking into account the emission wavelengths of other SL TMDs such as WS_2 ($\lambda_{em} \sim 630$ nm) and SL $MoSe_2$ ($\lambda_{em} \sim 729$ nm), the interference model predicts the same substrates would also be a good choice for an excitation wavelength of 532 nm. Overall, 110 nm of SiO_2 is the best choice to optimize simultaneously the PL of the most popular 2D TMDs.

Such environmental-induced effects have also been observed for the G and 2D Raman signals of graphene [29–31] and the Raman modes of TMDs [32–34], as summarized in Figures S5 and S6 (see Supplementary Information). Again, the MST accurately accounts for the Raman intensities of the G and 2D modes of SL graphene (Figure S5a) and the A_{1g} and E^1_{2g} modes of SL MoS_2 (Figures S6a and S6b, respectively) as a function of the SiO_2 thickness. Figure S6c (Supplementary Information) shows the Raman intensity of the E^1_{2g} mode measured in MoS_2 nanoflakes of different thicknesses supported on SiO_2/Si substrates, as extracted from Ref. [32]. The good match observed between experimental results and the trend obtained by means of the MST indicates that the model also accurately accounts for the variation of the Raman intensity signals due to changes in the thickness of the active material.

3 Source term method for the design of multilayer devices with optimized response

The good agreement between experimental and calculated values obtained for the PL of SL MoS_2 indicates that the MST provides for a very versatile and accurate tool for designing multilayer devices using 2D TMDs as an active material with an optimized response. Limiting ourselves to the case of MoS_2, we have calculated PL intensities of SL MoS_2 deposited on different multilayer structures (these schematized in Figure 4A). In the calculations, excitation and emission wavelengths of 632 and 670 nm have been selected, respectively. A NA of 0.9 for the collection objective has also been considered. All calculated PL intensities have been normalized to that of a free-standing SL of MoS_2. Following this normalization procedure, an easy and reliable comparison pattern can be established among the structures proposed here, and these eventually proposed in other works. Figure 4B shows the calculated PL enhancement obtained for SL MoS_2 deposited in three different multilayer structures. For the extensively used

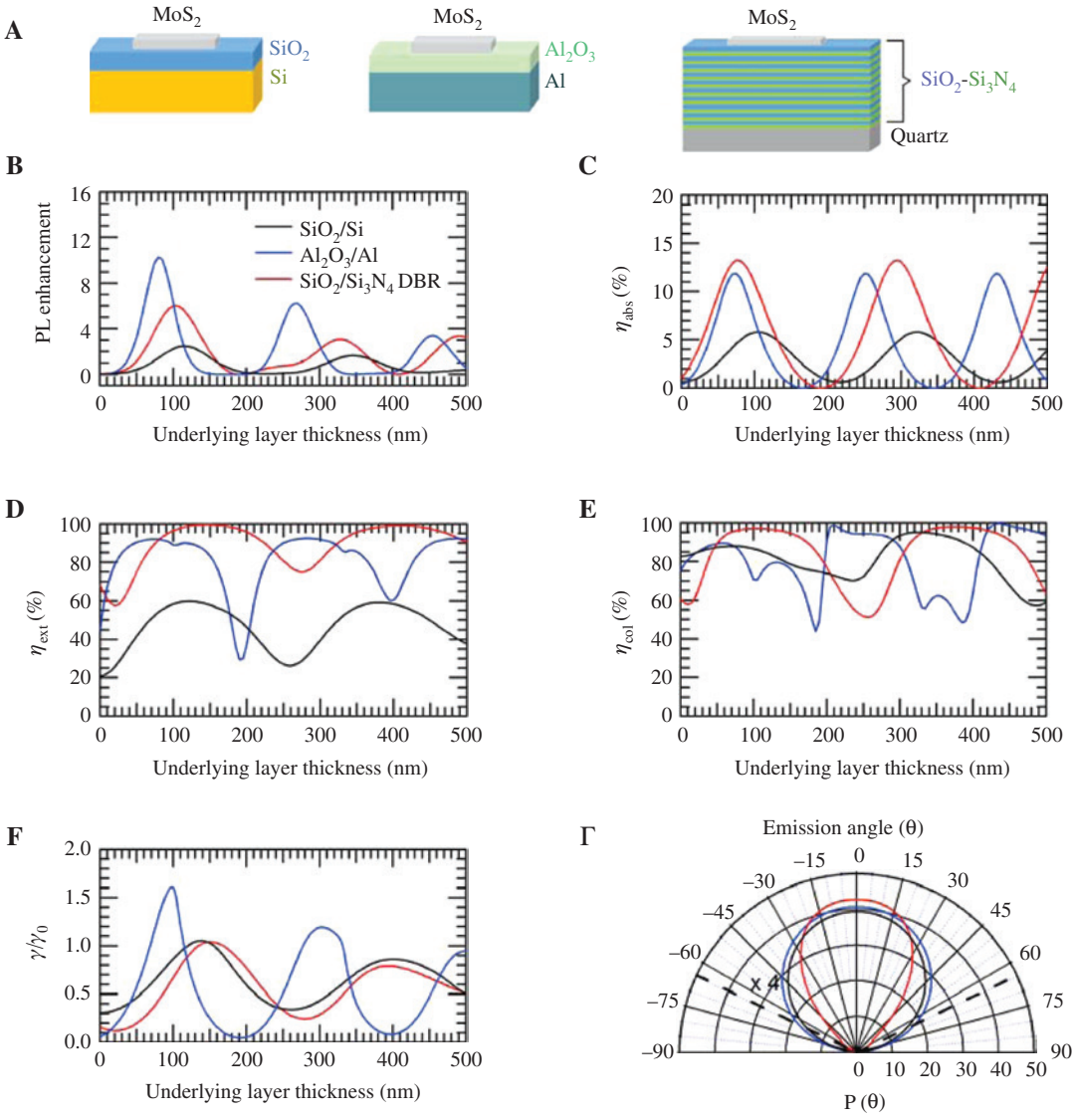

Figure 4: (A) Schematic illustration of the three different multilayer structures designed to enhance the PL response of MoS_2 SL. (B) Calculated enhancement of the PL of SL MoS_2 deposited on these multilayer structures. (C) Calculated absorption efficiency of the MoS_2 layer at the excitation wavelength corresponding to the curves shown (B). (D) Calculated variation of the extraction efficiency for the structures shown in (A). (E) Calculated variation of the collection efficiency for the structures shown in (A). (F) Calculated evolution of the spontaneous emission rate modification for MoS_2 deposited on three different substrates as a function the underlying thickness. (G) Calculated power radiated per unit solid angle in the far field corresponding to the conditions for which the maximum PL enhancement is achieved for each multilayer structure in Figure 4A.

Si/SiO_2 substrates, a maximum PL enhancement of 2.4 is observed when a SiO_2 underlayer of ~110-nm thick is used (as discussed above). Alternative multilayer structures have been proposed to enhance the PL signal of MoS_2, such as an alumina spacer sandwiched between SL MoS_2 and an aluminum reflector [42]. For these structures, we find that a maximum PL enhancement of ~10 is obtained for alumina layers ~80-nm thick. Additionally, two less intense peaks with PL enhancements of ~6.2 and ~3.4 are observed for 265 and 450 nm of alumina, respectively. The higher PL enhancements obtained for this multilayer structure have their origin mainly in the higher reflectivity of the Al_2O_3/Al interface for both excitation and emission wavelengths in comparison to that of SiO_2/Si. The third substrate we consider consists of a multilayer structure in which the MoS_2 sheet is deposited onto a more sophisticated mirror-like dielectric structure such as a flat distributed Bragg reflector (DBR). Such a DBR structure has been designed to consist of ten pairs of $\lambda/4$ (λ being the light wavelength) SiO_2/Si_3N_4 layers placed above a quartz

substrate. The thickness of the oxide layers has been chosen to achieve optimized reflectivity at both excitation and emission wavelengths. The PL enhancement expected for SL MoS_2 deposited on such a DBR structure has been calculated as a function of the thickness of the underlying SiO_2 layer (red solid line in Figure 4B). For this DBR structure, three maximum PL enhancements of ~6, ~3, and ~3.4 are predicted for SiO_2 thicknesses of 102, 330, and 490 nm, respectively. At this point, we would like to stress that the maximum PL enhancement values obtained here for the above proposed SiO_2/Si, Al_2O_3/Al, and DBR structures have been normalized by using PL intensity values expected for a free-standing SL as a reference. Other authors have selected to use the PL intensity of a MoS_2 SL on top of Si substrate as normalization factor [48] and then claiming to obtain extremely high PL enhancement values. We consider that such a normalization choice (by using MoS_2 on Si substrates) gives rise to artificially high PL enhancement values due to the fact that the PL signal of MoS_2 on Si substrates becomes strongly quenched with respect to that of the free-standing 2D layer [48]. In fact, if we had used such a normalization factor for our calculations, the PL enhancement expected for MoS_2 on SiO_2/Si, Al_2O_3/Al and DBR structures would be as high as ~100, ~400, and ~250, respectively. However, information on real benefits of using these proposed structures to enhance the intrinsic PL response of MoS_2 SL would have been missed.

In general, environment-related optical interference effects can be observed in the PL signal of MoS_2 for the three structures considered in the calculations (Figure 4B). When considering the dipolar nature of the optical emission processes, such a modulation of the PL emission can be understood again as the combination of different factors. Following the discussion adopted in Ref. [42], the measured PL power can be estimated by the following equation:

$$P_{PL} \propto \eta_{abs}\eta_{ext}\eta_{col}\eta_q P_{exc}, \quad (1)$$

with P_{PL} and P_{exc} being the measured and excitation powers, respectively. η_{abs}, η_{ext}, η_{col}, and η_q represent the absorption, extraction, collection, and quantum efficiencies, respectively. The first term in Eq. (1) (η_{abs}) refers to the interference effect present for the optical absorption in the 2D material due to the multiple reflections in the multilayer structure, as discussed previously. The second one (η_{ext}) accounts for the ratio of power emitted to the air with respect to the total radiated power by the dipole. The third term (η_{col}) accounts for the ratio of collected power in the far-field with respect to the total radiated power to the air. Regarding to the quantum efficiency η_q, it can be approximated by $\eta_q = \gamma(\gamma+\gamma_{nr})^{-1} \approx \gamma\gamma_{nr}^{-1}$, with γ and γ_{nr} being the radiative and non-radiative recombination rates ($\gamma \ll \gamma_{nr}$), respectively [42]. Such an approximation is valid because the exciton decay time of 2D materials at room temperature is typically dominated by non-radiative recombination [49]. The measured power can thus be estimated by the following equation:

$$P_{PL} \propto \eta_{abs}\eta_{ext}\eta_{col}\gamma\gamma_{nr}^{-1}P_{exc}. \quad (2)$$

This means that, for a given excitation power and γ_{nr}, the optimization of the PL power in the far field can be achieved by maximizing the product $\eta_{abs}\eta_{ext}\eta_{col}\gamma$, as stated by Eq. (2).

Following Eq. (2), the calculated variation of the total emitted power as a function of the underlying layer thickness shown in Figure 4B can be decomposed into different contributions. Figure 4C shows the absorption efficiency at the excitation wavelength (η_{abs}) of the SL MoS_2 corresponding to the curves shown in Figure 4B as a function of the thickness of the underlying layer. As it can be seen in this figure, similar maximum absorption efficiencies of ~12% and ~13% are obtained for the Al_2O_3/Al and bottom DBR structures, which turned out to be more than a factor 2 higher than that obtained for SiO_2/Si (6%). Such a difference in η_{abs} has its origin in the higher reflectivity of the Al_2O_3/Al and DBR structures at the excitation wavelength in comparison to that of SiO_2/Si. Figure 4C and D shows a strong dependence of η_{ext} and η_{col} with the thickness of the underlying layer for the three multilayer structures, whose origin lies in their corresponding angular redistribution of photons. We note that from Figure 4C–E, it can be observed that the product of the variations of η_{abs}, η_{ext}, and η_{col} does not account by itself for the calculated variations of the PL for each structure shown in Figure 4B, indicating that the spontaneous emission rate γ of the dipole is also being modified by the planar structures. The MST also allows estimating the modification of the spontaneous emission rate γ/γ_0 by using Eq. (S8) in the Supplementary Information (see Figure 4F for the calculated variation of γ/γ_0 in the three structures). The maximum estimated values of γ/γ_0 are ~1.6, ~1.05, and ~1.05 for the Al_2O_3/Al, the DBR, and the SiO_2/Si structures, respectively. The higher values of γ/γ_0 observed for the Al_2O_3/Al can be attributed to the higher reflectivity of the Al for a wide angular range in comparison to the DBR and Si and the higher penetration depth of the mode for the case of the DBR structure.

For completeness, Figure 4G shows the calculated power radiated per unit solid angle in the far field corresponding to the conditions for which the maximum PL enhancement is achieved for each multilayer structure shown in Figure 4A. These results show that such structures produce very different angular patterns. The most

directional one is obtained when MoS_2 is placed on top of a SiO_2/Si_3N_4 DBR. Such a higher directionality has its origin in the angular dependence of the reflectivity of the DBR. While DBRs are able to provide high reflectivity at normal incidence, light at larger angles can leak through the mirror. Obviously, the Al mirror exhibits high reflectivity independently of the incident angle.

Bearing in mind the different factors that contribute to the collected PL in the far field, the MST can be applied to design and optimize multilayer structures with higher technological projection than those shown in Figure 4A. We find a maximum PL enhancement of ~30 if the MoS_2 SL is placed inside a SiO_2 microcavity sandwiched between two mirrors. The top mirror is a DBR that consists of eight pairs of SiO_2/Si_3N_4, while the bottom mirror is a gold reflector. The number of pairs and the thickness of the SiO_2 and Si_3N_4 layers in the top mirror have been chosen to achieve a moderate reflectivity for the excitation wavelength (in order to both allow an efficient excitation and to increase the excitation electric field at the MoS_2 plane) and a high transmission at the emission wavelength. MoS_2 is placed in the middle of a SiO_2 central layer of thickness of $\lambda_{em}/(2n)$, with λ_{em} and n being the emission wavelength of SL MoS_2 and the refractive index of the SiO_2 layer, respectively. Following Eq. (2), we can again decompose the total collected PL signal intensity into different contributions. Calculations reveal that, for this particular multilayer structure, the absorption efficiency of the 2D material at the excitation wavelength can be increased up to 52%. Regarding extraction efficiency, calculations indicate that it decreases down to ~30%. The effect of embedding the 2D material in a cavity in addition to the presence of the top DBR leads to a diminution of the number of photons that are able to escape to the air (due to total internal reflection) in comparison to the structures discussed previously, where MoS_2 was directly radiating to the air. However, once the photons have been extracted from the cavity to the air, ~90% of the emitted power can be collected by an objective lens with NA = 0.9, demonstrating good emission directionality. Finally, a γ/γ_0 of ~2.5 has been estimated for this structure, which indicates that the increase of the PL enhancement observed for this multilayer structure has its origin mainly in a combination of the increase of η_{abs} and an enhancement of the spontaneous emission rate by Purcell effect [50].

Apart from being able to provide a versatile tool to design multilayer devices using 2D TMDs with optimized response, the versatility of the MST in comparison to the multiple reflection models becomes evident when dealing with 2D materials with eventual out-of-plane dipoles. On the one hand, this issue is important for 2D semiconductors different from 2D TMDs [46]. In fact, the nature of the orbitals involved in the optical bandgap and the dipolar selection rules for optical transitions of 2D InSe – a semiconductor with a highly tunable band gap [35, 51] – suggest that InSe could be an example of a 2D material with an important out-of-plane dipole contribution. On the other hand, the design of multilayer structures with optimized light extraction capabilities (independently of their dipole orientation) is also relevant for 2D TMDs, as it may allow to relax nearly flat requisites of devices based on these materials to provide an optimal response.

In the following, we demonstrate the versatility of the MST in the design of multilayer structures showing nearly 100% extracted photon flux ($\eta_{ext}\eta_{col}$) of the emitted power for 2D semiconductors independently of their dipole orientation. Figure 5A shows a sketch of the proposed structure. Similar multilayer structures were proposed by Chen et al. [52] to enhance the extraction efficiency of the zero-phonon line of the nitrogen-vacancy color center in diamond. The structure consists of a thick sapphire capping layer on top of a PMMA layer with thickness t deposited on top of a LiF spacer with thickness s deposited over a gold reflector. The 2D nanoflake is embedded in the PMMA layer at a distance d from the sapphire/PMMA interface, and the emitted power can then be collected using an immersion objective with an immersion oil index matched with the sapphire capping layer. Figure 5B shows a contour plot where the calculated extracted photon flux in a cone with an angle of 136° (NA = 1.65) is plotted as a function of t and the d/t ratio for 2D materials with horizontal (upper panel) and vertical (lower panel) dipoles. Calculations have been done for a selected emission wavelength of ~700 nm and a LiF spacer thickness of $s = 200$ nm, which ensures a low coupling to surface plasmon polariton (SPP) modes in the metal/dielectric interface [52]. It is worth noting that, as in the rest of the work, we have not considered the possible reabsorption of the emitted light by the 2D nanoflakes. As it can be observed in this figure, it is possible to collect over 90% of the emitted power almost independently of the dipole orientation, the PMMA thickness, and the vertical position of the 2D material within the PMMA layer, which indicates that, under real fabrication processes, the PMMA layer thickness value selected is not a critical parameter. A small decrease of the extraction efficiency can be observed for low d/t ratios. Such a decrease has its origin in the progressive increase of the coupling of the dipole evanescent field to the higher refractive index layer (Sapphire) as d is reduced. This evanescent field becomes propagative in the high-index medium, and it propagates at angles above the critical angle, escaping the NA of the collection objective.

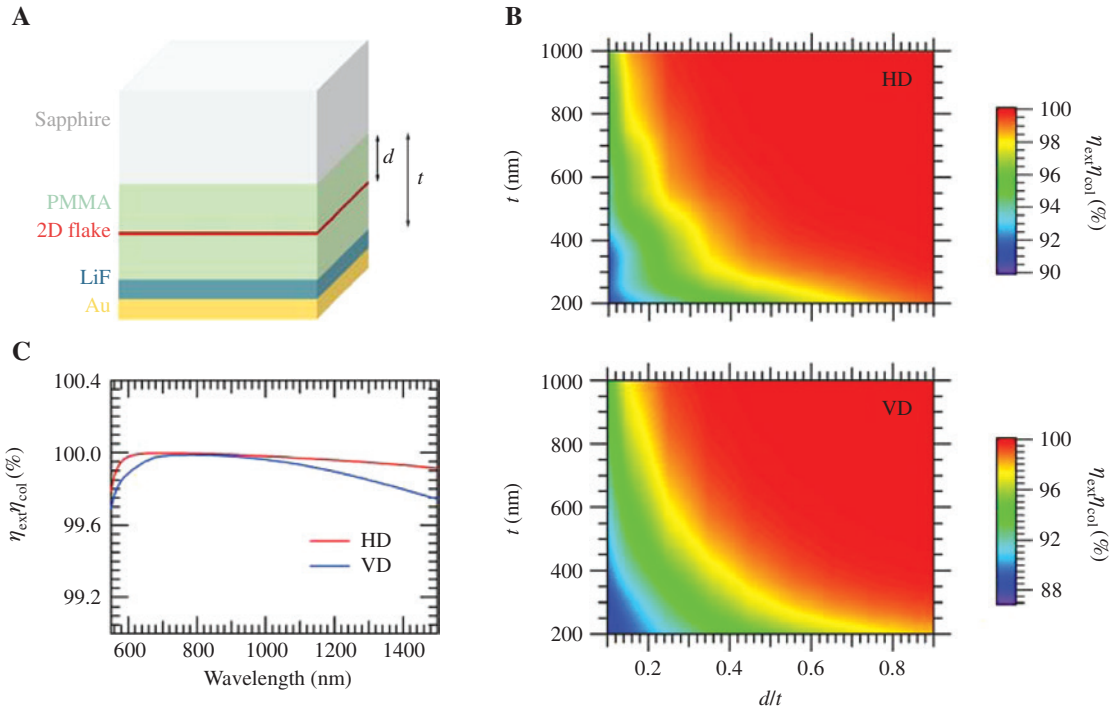

Figure 5: (A) Schematic illustration of the multilayer structure proposed to enhance the extracted photon flux for 2D materials. (B) Calculated extracted photon flux efficiency for 2D materials with horizontal (HD, upper panel) and vertical (VD, lower panel) dipoles emitting at $\lambda = 700$ nm. (C) Calculated extracted photon flux efficiency for 2D materials embedded at a distance $d = 640$ nm in an 800-nm-thick PMMA layer as a function of the emission wavelength.

The light extraction advantages of the multilayer structure proposed above are restricted not only to a particular 2D material emitting at ~700 nm but also to those emitting in the entire emission range provided, for instance, by 2D TMDs, phosphorene, and 2D InSe. Figure 5C shows the calculated extracted photon flux for 2D materials embedded at a distance $d = 640$ nm in an 800-nm-thick PMMA layer as a function of the emission wavelength. As it can be observed in this figure, calculations predict that over 99% of the light emitted by these 2D materials can be collected by a NA = 1.65 independently of the emission wavelength and the dipole orientation. These results are relevant for the design of real devices based on 2D materials with optimal photon flux extraction in which surface roughness or fabrication processes would introduce a certain dipole misalignment degree.

4 Optimizing single-photon extraction in 2D WSe_2 and h-BN

So far, we have shown that PL emission from exciton recombination in 2D TMDs can be tuned by an appropriate choice of the substrate. However, it has been recently reported that crystal structure imperfections or disorder in some 2D materials such as WSe_2 [10–14] and h-BN [15–17] can act as efficient carrier trapping centers that behave as SPEs. In this section, we use the modified MST for the study of the conditions that maximize the extraction of quantum light in 2D WSe_2 and h-BN deposited on SiO_2/Si and Al_2O_3/Al substrates. The 2D nature of these SPEs confined to atomically thin materials allows the enhancement of photon-extraction efficiency and facilitates a controllable external modification because of the proximity of the SPEs to the material surface.

It has been observed that these SPEs usually present a saturation behavior for low excitation powers [10, 12–15]. The saturation power varies for different emitters, but saturation is always observed for excitation powers that can be easily achieved experimentally, which reduces the importance of the role of the absorption efficiency in the single-photon emission process. For this reason, in these particular calculations, we have not considered the contribution of the absorption efficiency to the total emitted intensity. Figure 5A shows a color map in which the source term method has been applied to calculate the collected emission intensity of SPE in SL WSe_2 deposited on a SiO_2/Si substrate. The SPEs have been modeled as horizontal dipoles. The color map

shows the dependence of the collected PL intensity as a function of the thickness of the underlying SiO_2 and the SPE emission wavelength. The range of emission wavelength for the SPEs has been considered to be between 720 and 810 nm [14], again considering in the calculations a NA = 0.9. Two regions of high single-photon emission appear for SiO_2 thicknesses of ~150 and ~440 nm, with the 150-nm SiO_2 thickness yielding the optimum performance. Figure 6A also indicates that SiO_2 thicknesses between 240 and 340 nm are not a good choice to enhance single-photon emission. The single-photon collection efficiency is higher than 80% for both 150 and 440 nm of SiO_2 thickness, practically independent of the emission wavelength, as observed in Figure 6B. Insets in Figure 6B show the far-field emission patterns of SPEs radiating at 760 nm for both 150 (left) and 440 nm (right) SiO_2 thicknesses.

Figure 6C shows results for an Al_2O_3/Al substrate. In this case, the two bands of high single-photon emission intensity appear for Al_2O_3 thicknesses of ~100 and ~340 nm, with the 100-nm Al_2O_3 thickness yielding the highest single-photon emission intensity. Results shown in Figure 6A and C indicate that the Al_2O_3/Al substrate outperforms the SiO_2/Si structure in terms of collected intensity by more than a factor of ~2. The calculated single-photon collection efficiency for 100 nm of Al_2O_3 is ~80% independent of the emission wavelength, whereas for 340 nm of Al_2O_3, an increase of the collection efficiency from ~75% up to 93% is observed in Figure 6D for increasing emission wavelength. The far-field emission pattern of a horizontal SPE radiating at 760 nm for 100 nm and 340 nm Al_2O_3 thicknesses is shown in the left and right insets of Figure 6D, respectively.

Figure S7 in the Supplementary Information shows similar calculations in which the MST has been applied to calculate the emission intensity of SPE in 2D h-BN deposited on SiO_2/Si and Al_2O_3/Al substrates. These results indicate that SiO_2 thicknesses of 130 and 350 nm and Al_2O_3 thicknesses of 90, 290, and 450 nm are the best thicknesses to optimize the single-photon emission intensity of 2D h-BN in the whole emission spectral range. Moreover, our results also evidence that the Al_2O_3/Al substrate outperforms the SiO_2/Si substrate in terms of emission intensity by a factor of ~2.

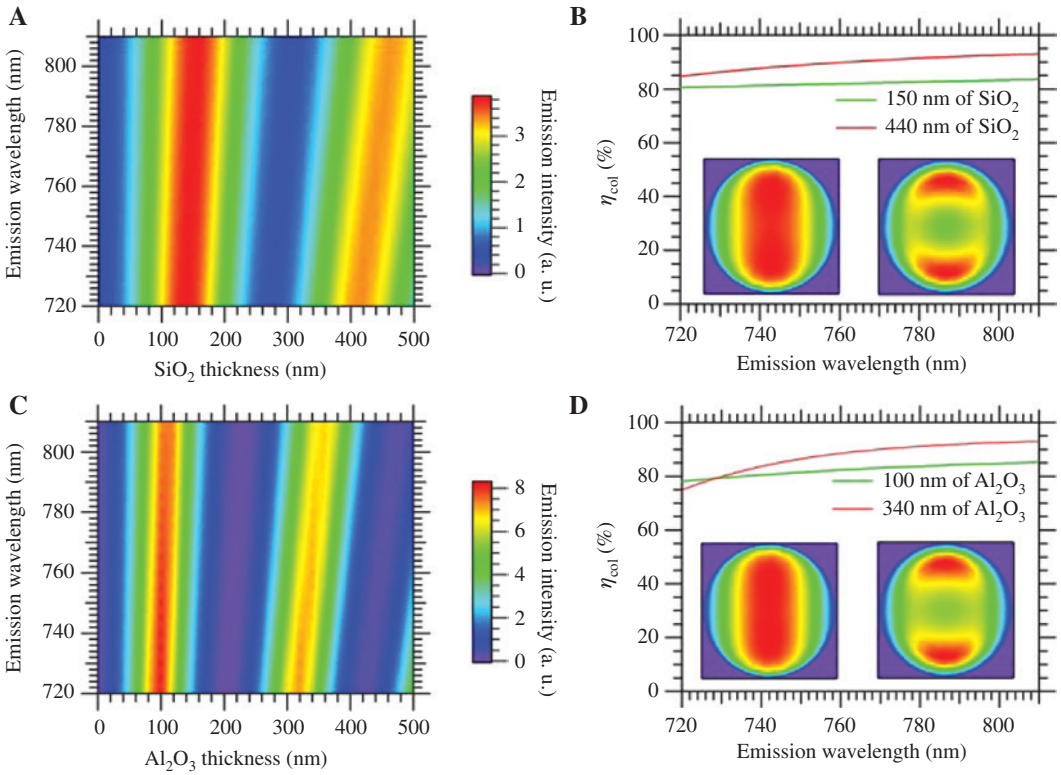

Figure 6: (A) Calculated single-photon emission intensity in SL WSe_2 deposited on a SiO_2/Si substrate as a function of the emission wavelength and the SiO_2 thickness. (B) Calculated single-photon collection efficiency for SiO_2 thicknesses of 150 and 440 nm. The insets show the far-field emission patterns of SPEs radiating at 760 nm for both 150 (left) and 440 nm (right) SiO_2 thicknesses. (C) Calculated single-photon emission intensity in SL WSe_2 deposited on Al_2O_3/Al substrate as a function of the emission wavelength and the Al_2O_3 thickness. (D) The insets show the far-field emission patterns of SPEs radiating at 760 nm for both 100 (left) and 340 nm (right) Al_2O_3 thicknesses.

The results shown in this section indicate that the single-photon emission in 2D materials can be easily optimized by modifying the underlying substrate. These properties, together with the full compatibility of 2D materials with integrated photonics approaches, position these materials as suitable candidates for the development of new quantum photonic devices in planar architectures.

5 Microcavity polaritons in 2D MoS_2

As already discussed, the interaction of a dipole with light can be tuned by an appropriate choice of the surrounding dielectric environment. In this way, the spontaneous emission rate and direction of emission of the dipole can be modified by embedding the dipole in an optical cavity. These effects have been experimentally demonstrated for 2D MoS_2 using photonic crystal cavities [53]. In that work, the authors reported an experimental Purcell enhancement of the MoS_2 spontaneous emission rate exceeding a factor of 70. However, the interaction rate between the dipole and the cavity photons was slower than the average dissipation rates and hence defined to be in the weak coupling regime [18].

When the interaction between the dipole and the cavity photons occurs at a rate that is faster than the average dissipation rates of the cavity photon and dipole, one enters the strong coupling regime, resulting in the formation of new eigenstates that are half-light, half-matter bosonic quasiparticles called cavity polaritons. Recently, Liu et al. [18] have reported the experimental evidence of strong light-matter coupling and the formation of microcavity polaritons in 2D MoS_2 embedded inside a dielectric microcavity at room temperature. A Rabi splitting of 46 ± 3 meV has been observed in angle-resolved reflectivity and PL spectra due to coupling between the 2D excitons and the cavity photons. It is well known that the energy dispersion of microcavity polaritons observed via reflectivity measurements can be simulated in the framework of both a semiclassical and a full quantum theory [54, 55]. In the quantum mechanical approach, the Rabi splitting and the spontaneous emission rate of the excitons are found by perturbation theory as a result of the interaction between two effective harmonic oscillators representing an exciton and a confined photon mode [56, 57]. The semiclassical theory is based on a nonlocal susceptibility treatment of the optical response of the active material [58, 59], with the advantage that it can be easily combined with a conventional transfer matrix formalism [55, 60]. Here, we show that the MST can be used to simulate the energy dispersion of microcavity polaritons in 2D materials embedded in multilayer planar structures. The transfer matrix nature of the MST and its straightforward numerical implementation make this method a suitable tool for the study of the formation of cavity polaritons in 2D materials embedded in optical planar cavities, which can play an important role in the design of new polaritonic devices operating at room temperature.

Following the experimental work in Ref. [18], we consider a microcavity consisting of SL MoS_2 placed in the middle of a SiO_2 cavity of thickness $\lambda_{cav}/(2n)$, where λ_{cav} represents the wavelength of the cavity mode at normal incidence and n represents the SiO_2 refractive index. This structure is then placed between two SiO_2/Si_3N_4 DBR mirrors, with 7.5 and 8.5 SiO_2/Si_3N_4 periods for the upper and lower mirrors, respectively. The dielectric constant of the 2D material has been modeled by a two-Lorentzian oscillator based on experimental data, where the half-width at half-maximum of the A exciton of the MoS_2 turns out to be $\hbar\Gamma_{exA} = 30$ meV [18, 61]. The emission of the 2D material has been modeled as a Lorentzian function with a half-width at half-maximum of 30 meV centered at the energy of the A exciton [18].

Figure 7A shows a color map of the calculated angle-resolved PL intensity obtained for the described microcavity with an initial (i.e. from fabrication) detuning Δ of −40 meV for the TM polarization. The results for TE polarization (not shown) are almost identical. The detuning is defined as $\Delta = E_{cav} - E_{excA}$, with E_{cav} and E_{excA} being the cavity mode and exciton energies, respectively. Figure 7A also shows the energy of the A exciton (red dashed line) and the calculated dispersion of the cavity mode (black dashed line). As a result of the strong coupling between the A exciton of MoS_2 and the cavity photons, two emission bands identified as the lower polariton branch and the upper polariton branch appear centered at energies different from E_{excA} and E_{cav}. For each collection angle, the resulting PL spectrum can be fitted to two Lorentzian peaks with quite good agreement. The energy positions of these two emission bands are also shown in Figure 7A by black dots. The lower polariton branch blue shifts with increasing angle and approaches E_{excA}, while the upper polariton branch shifts away from E_{excA} with increasing angle, showing a clear anticrossing behavior between the A exciton and the cavity mode. Figure 7B shows a similar calculation for a microcavity where the initial detuning was set to $\Delta = -10$ meV. Rabi splittings of $\hbar\Omega_{Rabi} = 46$ meV and 48 meV can be estimated from the energy splitting of the peaks at the anticrossing angles for the cavities with detunings of −40 and −10 meV, respectively. These estimated values of $\hbar\Omega_{Rabi}$ are in good agreement with the

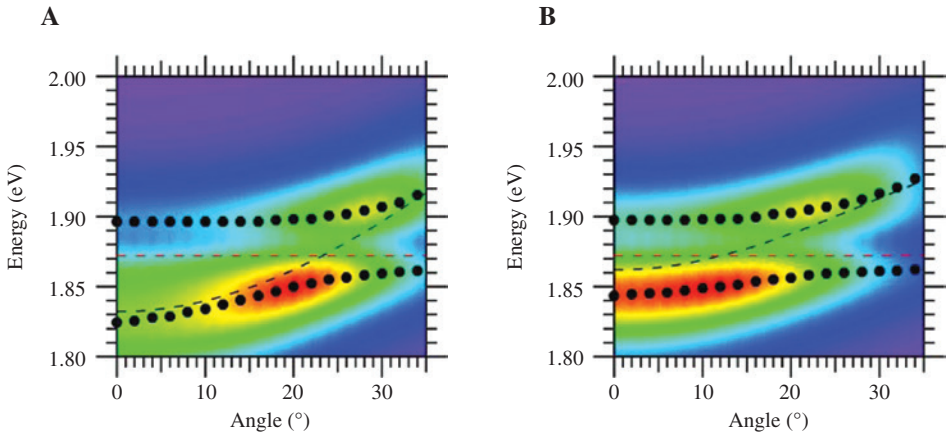

Figure 7: Simulated color map of the angle-resolved PL intensity from the 2D MoS_2 for microcavities with a detuning of −40 meV (A) and −10 meV (B) showing exciton-polariton anticrossing at different angles.

experimental values observed for 2D MoS_2 in similar cavities [18]. These results demonstrate that the MST model is very useful to study the energy dispersion of microcavity polaritons of 2D MoS_2 in optical vertical cavities in the strong coupling regime and hence a suitable tool to design future photonic devices based on 2D materials.

6 Conclusions

In this work, we have applied the transfer matrix-based source term method to study and optimize PL and Raman processes in 2D materials such as MoS_2 and graphene, among other 2D materials. Significantly, we incorporate the effects of the excitation process (e.g. absorption) in the model, which is needed to optimize the PL intensity of SL MoS_2 on different multilayer structures. Among the multilayer structures tested, an alumina layer with a thickness of ~80 nm deposited on the top of an aluminum reflector has been demonstrated to be the simplest substrate that can be used to maximize the PL intensity of SL MoS_2 for an excitation wavelength of 632 nm. Further, we have demonstrated an enhancement of the PL intensity by a factor of ~30 if the SL MoS_2 is placed inside a SiO_2 cavity sandwiched between a DBR and a gold reflector, which act as the top and bottom mirrors, respectively. Similar studies can be performed on other 2D dichalcogenides. Additionally, we have found that multilayer structures can be designed to enhance the extracted photon flux for a large variety of 2D materials. Also, we have shown that the single-photon emission in 2D materials such as WSe_2 and h-BN can be enhanced by an appropriate choice of the underlying substrate. These results, together with the full compatibility of 2D materials with integrated photonics approaches, position these materials as strong candidates for the development of new quantum photonic devices. Finally, the model has been used to simulate the energy dispersion of microcavity polariton formation in 2D MoS_2, which nicely fitted the experimentally reported data. Our results indicate that the source term method is a highly versatile and accurate analytical tool for modeling and optimizing light emission of 2D systems and related devices in both the weak and the strong coupling regimes. Its transfer matrix nature, together with its straightforward numerical implementation, make this method a useful tool for the study of light emission of 2D materials embedded in optical planar cavities, which can play a relevant role for the design of new polariton devices operating at room temperature.

Acknowledgments: This work was supported by the Spanish Government (grant nos. TEC2014-53727-C2-1-R), the Comunidad Valenciana Government (grant no. PROMETEOII/2014/059), the Engineering and Physical Sciences Research Council (EPSRC) (EP/I023186/1, EP/K015338/1, EP/L015110/1), and the European Research Council (ERC) (no. 307392). M. B. G. acknowledges fellowship no. UVINV-PREDOC13-110538 under the program "Atracció de Talent, VLC-CAMPUS" of the University of Valencia. B.D.G. thanks the Royal Society for a University Research Fellowship. The authors acknowledge the fruitful discussions with Professor Alfredo Segura.

References

[1] Butler SZ, Hollen SM, Cao L, et al. Progress, challenges, and opportunities in two-dimensional materials beyond graphene. ACS Nano 2013;7:2898–926.

[2] Bhimanapati GR, Lin Z, Meunier V, et al. Recent advances in two-dimensional materials beyond graphene. ACS Nano 2015;9:11509–39.
[3] Jones AM, Yu H, Ghimire NJ, et al. Optical generation of excitonic valley coherence in monolayer WSe_2. Nat Nanotechnol 2013;8:634–8.
[4] Poellmann C, Steinleitner P, Leierseder U, et al. Resonant internal quantum transitions and femtosecond radiative decay of excitons in monolayer WSe_2. Nat Mater 2015;14:1–6.
[5] Bernardi M, Palummo M, Grossman JC. Extraordinary sunlight absorption and one nanometer thick photovoltaics using two-dimensional monolayer materials. Nano Lett 2013;13:3664–70.
[6] Splendiani A, Sun L, Zhang Y, et al. Emerging photoluminescence in monolayer MoS_2. Nano Lett 2010;10:1271–5.
[7] Mak KF, Lee C, Hone J, Shan J, Heinz TF. Atomically thin MoS_2: a new direct-gap semiconductor. Phys Rev Lett 2010;105:136805.
[8] Radisavljevic B, Radenovic A, Brivio J, Giacometti V, Kis A. Single-layer MoS_2 transistors. Nat Nanotechnol 2011;6:147–50.
[9] Sundaram RS, Engel M, Lombardo A, et al. Electroluminescence in single layer MoS_2. Nano Lett 2013;13:1416–21.
[10] Tonndorf P, Schmidt R, Schneider R, et al. Single-photon emission from localized excitons in an atomically thin semiconductor. Optica 2015;2:347.
[11] Koperski M, Nogajewski K, Arora A, et al. Single photon emitters in exfoliated WSe_2 structures. Nat Nanotechnol 2015;10:503–6.
[12] He YM, Clark G, Schaibley JR, et al. Single quantum emitters in monolayer semiconductors. Nat Nanotechnol 2015;10:497–502.
[13] Srivastava A, Sidler M, Allain AV, Lembke DS, Kis A, Imamoğlu A. Optically active quantum dots in monolayer WSe_2. Nat Nanotechnol 2015;10:491–6.
[14] Kumar S, Kaczmarczyk A, Gerardot BD. Strain-induced spatial and spectral isolation of quantum emitters in mono- and bilayer WSe_2. Nano Lett 2015;15:7567–73.
[15] Tran TT, Bray K, Ford MJ, Toth M, Aharonovich I. Quantum emission from hexagonal boron nitride monolayers. Nat Nanotechnol 2015;11:37–41.
[16] Chejanovsky N, Rezai M, Paolucci F, et al. Structural attributes and photodynamics of visible spectrum quantum emitters in hexagonal boron nitride. Nano Lett 2016;16:7037–45.
[17] Jungwirth NR, Calderon B, Ji Y, Spencer MG, Flatté ME, Fuchs GD. Temperature dependence of wavelength selectable zero-phonon emission from single defects in hexagonal boron nitride. Nano Lett 2016;16:6052–7.
[18] Liu X, Galfsky T, Sun Z, Xia F, Lin E. Strong light-matter coupling in two-dimensional atomic crystals. Nat Photonics 2015;9:30–4.
[19] Flatten LC, He Z, Coles DM, et al. Room-temperature exciton-polaritons with two-dimensional WS_2. Sci Rep 2016;6:33134.
[20] Dufferwiel S, Schwarz S, Withers F, et al. Exciton-polaritons in van der Waals heterostructures embedded in tunable microcavities. Nat Commun 2015;6:8579.
[21] Kern J, Trügler A, Niehues I, et al. Nanoantenna-enhanced light-matter interaction in atomically thin WS_2. ACS Photonics 2015;2:1260–5.
[22] Lee KCJ, Chen Y-H, Lin H-Y, et al. Plasmonic gold nanorods coverage influence on enhancement of the photoluminescence of two-dimensional MoS_2 monolayer. Sci Rep 2015;5:16374.
[23] Sobhani A, Lauchner A, Najmaei S, et al. Enhancing the photocurrent and photoluminescence of single crystal monolayer MoS_2 with resonant plasmonic nanoshells. Appl Phys Lett 2014;104:11–5.
[24] Najmaei S, Mlayah A, Arbouet A, Girard C, Léotin J, Lou J. Plasmonic pumping of excitonic photoluminescence in hybrid MoS_2-Au nanostructures. ACS Nano 2014;8:12682–9.
[25] Lee B, Park J, Han GH, et al. Fano resonance and spectrally modified photoluminescence enhancement in monolayer MoS_2 integrated with plasmonic nanoantenna array. Nano Lett 2015;15:3646–53.
[26] Butun S, Tongay S, Aydin K. Enhanced light emission from large-area monolayer MoS_2 using plasmonic nanodisc arrays. Nano Lett 2015;15:2700–4.
[27] Wang Z, Dong Z, Gu Y, et al. Giant photoluminescence enhancement in tungsten-diselenide–gold plasmonic hybrid structures. Nat Commun 2016;7:11283.
[28] Wu S, Buckley S, Jones AM, et al. Control of two-dimensional excitonic light emission via photonic crystal. 2D Mater 2014;1:11001.
[29] Wang YY, Ni ZH, Shen ZX, Wang HM, Wu YH. Interference enhancement of Raman signal of graphene. Appl Phys Lett 2008;92:043121.
[30] Yoon D, Moon H, Son Y-W, et al. Interference effect on Raman spectrum of graphene on SiO_2/Si. Phys Rev B 2009;80:125422.
[31] Liu C, Ma Y, Li W, Dai L. The evolution of Raman spectrum of graphene with the thickness of SiO_2 capping layer on Si substrate. Appl Phys Lett 2013;103:213103.
[32] Li S-L, Miyazaki H, Song H, Kuramochi H, Nakaharai S, Tsukagoshi K. Quantitative Raman spectrum and reliable thickness identification for atomic layers on insulating substrates. ACS Nano 2012;6:7381–8.
[33] Zhang H, Wan Y, Ma Y, Wang W, Wang Y, Dai L. Interference effect on optical signals of monolayer MoS_2. Appl Phys Lett 2015;107:101904.
[34] Lien D-H, Kang JS, Amani M, et al. Engineering light outcoupling in 2D materials. Nano Lett 2015;15:1356–61.
[35] Brotons-Gisbert M, Andres-Penares D, Suh J, et al. Nanotexturing to enhance photoluminescent response of atomically thin indium selenide with highly tunable band gap. Nano Lett 2016;16:3221–9.
[36] Sánchez-Royo JF, Muñoz-Matutano G, Brotons-Gisbert M, et al. Electronic structure, optical properties, and lattice dynamics in atomically thin indium selenide flakes. Nano Res 2014;7:1556–68.
[37] Benisty H, Stanley R, Mayer M. Method of source terms for dipole emission modification in modes of arbitrary planar structures. J Opt Soc Am A 1998;15:1192.
[38] Carlin JF, Royo P, Stanley RP, et al. Design and characterization of top-emitting microcavity light-emitting diodes. Semicond Sci Technol 2000;15:145.
[39] Ramuz M, Bürgi L, Stanley R, Winnewisser C. Coupling light from an organic light emitting diode (OLED) into a single-mode waveguide: toward monolithically integrated optical sensors. J Appl Phys 2009;105:084508.
[40] Ma Y, Kremer PE, Gerardot BD. Efficient photon extraction from a quantum dot in a broad-band planar cavity antenna. J Appl Phys 2014;115:023106.
[41] Bienstman P, Bockstaele R, Baets R. Rigorous electromagnetic analysis of dipole emission in periodically corrugated layers:

the grating-assisted resonant-cavity light-emitting diode. J Opt Soc Am 2002;19:871–80.
[42] Janisch C, Song H, Zhou C, et al. MoS_2 monolayers on nanocavities: enhancement in light–matter interaction. 2D Mater 2016;3:25017.
[43] Aad R, Blaize S, Bruyant A, Couteau C, Lérondel G. Enhancement of ultrathin film emission using a waveguiding active layer. J Appl Phys 2010;108:123111.
[44] Tran TT, Elbadawi C, Totonjian D, et al. Robust multicolor single photon emission from point defects in hexagonal boron nitride. ACS Nano 2016;10:7331–8.
[45] Lieb MA, Zavislan JM, Novotny L. Single-molecule orientations determined by direct emission pattern imaging. J Opt Soc Am B 2004;21:1210.
[46] Schuller JA, Karaveli S, Schiros T, et al. Orientation of luminescent excitons in layered nanomaterials. Nat Nanotechnol 2013;8:271–6.
[47] Budde H, Coca-López N, Shi X, et al. Raman radiation patterns of graphene. ACS Nano 2016;10:1756–63.
[48] Lee Y-C, Tseng Y-C, Chen H-L. Single type of nanocavity structure enhances light outcouplings from various two-dimensional materials by over 100-fold. ACS Photonics 2017;4:93–105.
[49] Shi H, Yan R, Bertolazzi S, et al. Exciton dynamics in suspended monolayer and few-layer MoS_2 2D crystals. ACS Nano 2013;7:1072–80.
[50] Purcell EM. Spontaneous emission probabilities at radio frequencies. Phys Rev 1946;69:681.
[51] Mudd GW, Svatek SA, Ren T, et al. Tuning the bandgap of exfoliated InSe nanosheets by quantum confinement. Adv Mater 2013;25:5714–8.
[52] Chen X-W, Goetzinger S, Sandoghdar V, Götzinger S, Sandoghdar V. 99% Efficiency in collecting photons from a single emitter. Opt Lett 2011;36:3545–7.
[53] Gan X, Gao Y, Fai Mak K, et al. Controlling the spontaneous emission rate of monolayer MoS_2 in a photonic crystal nanocavity. Appl Phys Lett 2013;103:1–5.
[54] Savona V, Andreani LC, Schwendimann P, Quattropani A. Quantum well excitons in semiconductor microcavities: unified treatment of weak and strong coupling regimes. Solid State Commun 1995;93:733–9.
[55] Ivchenko EL, Kaliteevski MA, Kavokin AV, Nesvizhskii AI, Ioffe AF. Reflection and absorption spectra from microcavities with resonant Bragg quantum wells. J Opt Soc Am B 1996;13:1061.
[56] Jorda S. Theory of Rabi splitting in cavity-embedded quantum wells. Phys Rev B 1994;50:18690–3.
[57] Jorda S. Spontaneous emission of quantum well excitons in planar dielectric multilayer cavities. Solid State Commun 1995;93:45–8.
[58] Andreani LC, Savona V, Schwendimann P, Quattropani A. Polaritons in high reflecticity microcavities: semiclassical and full quantum treatment of optical properties. Superlattices Microstruct 1994;15:453.
[59] Andreani LC. Exciton-polaritons in superlattices. Phys Lett A 1994;192:99–109.
[60] André R, Boeuf F, Heger D, et al. Cavity-polariton effects in II-VI microcavities. Acta Phys Pol A 1999;96:511–24.
[61] Hu T, Wang Y, Wu L, et al. Strong coupling between Tamm plasmon polariton and two dimensional semiconductor excitons. Appl Phys Lett 2017;110:51101.

Supplemental Material: The online version of this article (DOI: 10.1515/nanoph-2017-0041) offers supplementary material, available to authorized users.